

Experimental Study and Numerical Simulation of Tension and Stress Relaxation of Hot-Applied Sealant for Asphalt Pavement

Feng Li¹⁺, Yuan Zhou², Tinggang Li¹, Wei Zeng¹, and XianGuo Wang³

Abstract: Low temperature performance of hot-applied bituminous crack sealant is a key factor which influences the effect of asphalt pavement crack filling and sealing. In order to describe the constitutive stress-strain relationship at low temperature, experimental tests of extension and stress relaxation of crack sealants, are presented in this paper. The generalized Maxwell model is chosen for curve-fitting to determine the material model. Comparison of fitted curve and experimental results proves that the generalized Maxwell model in Prony series is well suited for describing the experiment process. Moreover, finite element analysis method with material model defined by the generalized Maxwell model in Prony series is introduced for numerical solution of tension and stress-relaxation of crack sealants. By comparing the results of the numerical analysis and the tests, the conclusion can be made that the tension and the stress-relaxation of crack sealants may be accurately depicted by the generalized Maxwell model.

DOI: 10.6135/ijprt.org.tw/2015.8(2).131

Key words: Curve fitting; Finite element analysis method; Generalized Maxwell model; Sealant; Visco-elastic.

Introduction

Crack sealing is considered one of the most cost-effective and frequently used maintenance techniques that may prolong the pavement service life. Crack sealing prevents the intrusion of water from penetrating into the pavement structure, hence, delays its deterioration. Over the life of the pavement, sealant should exhibit flexibility and extensibility at low service temperatures [1-2]. Hot-applied bituminous crack sealant is comprised of asphalt, rubber, extender oil, filler, and so on [3-4]. It may exhibit both viscous and elastic characteristics under deformation known as viscoelasticity.

To evaluate field performance, current specifications for hot-applied sealants are developed by ASTM D5329 [5], which provide test methods for sealants. The bond test, as one of these methods, is used to evaluate low temperature performance of sealants. ASTM D6690 [6] provides physical requirements for different types of sealant. The specification for hot-applied sealants in China [7] is similar to ASTM specifications. However, the current ASTM specifications for hot-applied sealants are empirical and cannot accurately predict their field performance. In order to develop test methods based on the material's rheological properties, numbers of experiments have been carried out to evaluate the low temperature performance of sealants, such as glass transition temperature, SHRP bending beam rheometer and direct tensile tester

[8-13].

Theory of viscoelasticity has been extensively studied for crack sealants under the stress relaxation tests. Using a Crack Sealant Bending Beam Rheometer, Elseifi [14] and Al-Qadi [15] developed a linear viscoelastic model to study the mechanical behavior of crack sealant at low service temperature. However, experimental study and numerical modeling of crack sealants during the process of constant strain rate loading and stress relaxation are seldom studied. This paper is focused on the experimental study and numerical simulation of crack sealants during the tension and the stress relaxation test. The generalized Maxwell model is chosen for curve-fitting to determine the material model. Finite element analysis method with material model defined by the generalized Maxwell model in Prony series is introduced for numerical solution of tension and stress-relaxation of crack sealants. By comparing the results of the numerical analysis and the tests, the tension and the stress-relaxation of crack sealants may be accurately depicted by the generalized Maxwell model.

Experiment Process

The test specimen, according to the bond test at low temperature of ASTM D5329 [5], is loaded under constant strain rate followed by stress relaxation. The test specimen is fastened with clamps and standing bolts, which are loaded through dowel steel (Fig. 1). The universal testing machine, combined with a cryogenic storage box and a computer, are used to measure the tensile stress. Crack sealant samples are stored in the cryogenic storage box for no less than 4 hours and then loaded with constant strain rate (0.02/h) till 25.6466% (labeled as sample 1) or 50% (labeled as sample 2) deformations take place. The time history of the stress is recorded afterwards, which means the experimental process is composed of two stages, namely the constant strain rate loading and the stress relaxation (Fig. 2). The temperature is kept at -30°C and the stress-time curves are automatically drawn by the computer.

¹ Key Laboratory of Road Structure and Material, Research Institute of Highway, Ministry of Transport, No. 8 Xitucheng Road, Haidian District, 100088, Beijing, China.

² Beijing Municipal Commission of Transport, No. 9A Liuliqiao South Road, Fengtai District, 100073, Beijing, China.

³ The Materials Department of the Transportation Bureau of Handan City, No. 56 Oxygen Road, Fuxing District, 056003, Handan, Hebei, China.

⁺ Corresponding Author: E-mail f.li@rioh.cn

Note: Submitted August 9, 2013; Revised February 13, 2015; Accepted February 17, 2015.

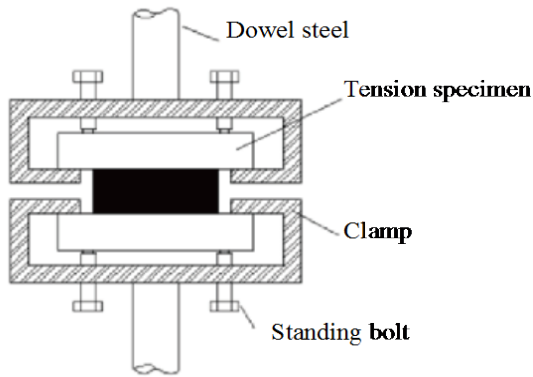


Fig. 1. Schematic Diagram of Extension Test.

Material Model

Crack sealants are tested under a simply uniaxial tensile loading at low temperature (-30°C), during which the strain rate is as low as 0.05 mm/min. As a result, the material model of crack sealants may be assumed to be small strain for each load step. At the end of the experiment procedure, 50% of the total deformation is achieved, which may be described by a large deformation process. In view of these two points, the theory of large deformation and small strain may be used for the material model of crack sealants under the constant strain rate loading and the stress relaxation. The standard linear solid model and the generalized Maxwell model are used for the description of the stress time history of crack sealants.

Prony Series [16]

Elastic modulus may be written in the form of Prony series, which is given by

$$E(t) = E(\infty) + \sum_{i=1}^k E_i \exp\left(-\frac{t}{\tau_i}\right) \tag{1}$$

$$= E(0) \left\{ 1 - \sum_{i=1}^k \alpha_i \left[1 - \exp\left(-\frac{t}{\tau_i}\right) \right] \right\}$$

where i represents the index of summation, k is the upper bound of summation, time dimension is denoted as t , elastic modulus is time-dependent and denoted as $E(t)$, and $E(\infty)$ is the long-term elastic modulus when the material is totally relaxed and α_i is the relative modulus given by

$$E(0)\alpha_i = E_i \tag{2}$$

Temperature effect on the relative modulus α_i and the relaxation time τ_i is assumed to be negligible since temperature is kept constant during the experiment procedure. The following conclusions may be drawn from Eq. (1).

- The material is thought to be purely elastic as time approaches zero. In this case, the elastic modulus may be initially evaluated by

$$E(0) = E(\infty) + \sum_{i=1}^k E_i \tag{3}$$

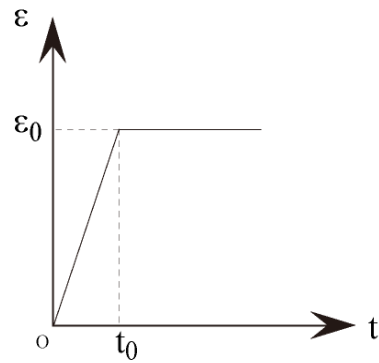


Fig. 2. Experimental Procedure.

- The elastic modulus is $E(\infty)$ and the material is thought to be near fluid as time approaches infinity.

Constitutive Relationship

The constitutive relationship may be formulated as [16]

$$\sigma = E(t)\epsilon_0 + \int_0^t E(t-\tau) \frac{d\epsilon}{d\tau} d\tau \tag{4}$$

where σ is stress, ϵ_0 is the strain at the initial time point. Eq. (4), written in the form of Prony series, may be recast into

$$\sigma = E(\infty)\epsilon + \sum_{i=1}^k E_i \exp\left(-\frac{t}{\tau_i}\right)\epsilon_0 + \int_0^t \left[\sum_{i=1}^k E_i \exp\left(-\frac{t-\tau}{\tau_i}\right) \right] \frac{d\epsilon}{d\tau} d\tau \tag{5}$$

Eq. (4) or Eq. (5) may be solved in accordance with the experiment steps shown in Fig. 3, namely constant strain rate loading and stress relaxation.

Constant Strain Rate Loading

The experimental sample is loaded under constant strain rate and Eq. (4) with zero initial strain may be solved by

$$\sigma = E(\infty)\dot{\epsilon}t + \sum_{i=1}^k E_i \dot{\epsilon}\tau_i \left[1 - \exp\left(-\frac{t}{\tau_i}\right) \right] \tag{6}$$

where a dot over the strain ϵ means the strain rate. The multiplication of two variables in the right-hand side of Eq. (6) may result in some divergent problems in case of curve-fitting. As a result, the viscosity coefficients are introduced here as

$$E_i \tau_i = \eta_i \tag{7}$$

Substituted by Eq. (7), Eq. (6) may be expressed as

$$\sigma = E(\infty)\dot{\epsilon}t + \sum_{i=1}^k \eta_i \dot{\epsilon} \left[1 - \exp\left(-\frac{t}{\tau_i}\right) \right] \tag{8}$$

The equation above is used for curve fitting to determine the unknown coefficients in Eq. (8) such as $E(\infty)$, η_i and τ_i , which are $2k+1$ in total numbers and may be approximated by the curve-fitting

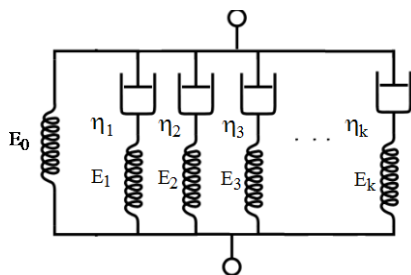


Fig. 3. Generalized Maxwell Model.

method. Two cases for the number of Maxwell elements in Fig. 4 are studied.

Stress Relaxation

At the second stage of the experiment, the stress relaxation of the sample is studied. The constitutive relationship, defined by Eq. (4) with the initial strain ϵ_0 at time t_0 , may be recalculated by

$$\sigma = \left[E(\infty) + \sum_{i=1}^k \frac{\eta_i}{\tau_i} \exp\left(-\frac{t-t_0}{\tau_i}\right) \right] \epsilon_0 \quad (9)$$

where the initial stress σ_0 at t_0 is

$$\sigma(t_0) = \sigma_0 = \left[E(\infty) + \sum_{i=1}^k \frac{\eta_i}{\tau_i} \right] \epsilon_0 \quad (10)$$

Therefore,

$$E(\infty)\epsilon_0 = \sigma_0 - \sum_{i=1}^k \frac{\eta_i}{\tau_i} \epsilon_0 \quad (11)$$

Eq. (9), substituted by Eq. (11), may be reformulated as

$$\sigma = \sigma_0 - \sum_{i=1}^k \frac{\eta_i}{\tau_i} \left[1 - \exp\left(-\frac{t-t_0}{\tau_i}\right) \right] \epsilon_0 \quad (12)$$

Two cases are examined for the number of Maxwell elements in Fig. 4.

Curve Fitting

The material model in Prony series as Eq. (5) is chosen for curve-fitting and the method of least squares is used to minimize the sum of the squared errors, which are defined by the difference between the experiment results $[\sigma]_j$ for the uniaxial stress and the solution σ_j predicted by the theoretical model as Eq. (5). The fitting procedure starts from minimizing the sum of the squares of the deviations f given by

$$f(E(\infty), \eta_i, \tau_i) = \sum_{j=1}^m (\sigma_j - [\sigma]_j)^2 \quad (13)$$

where $E(\infty)$ is the long-term elastic modulus when the material is totally relaxed, $[\sigma]_j$ is the experimental stress, m is the number of the experiment data set. The unknown coefficients, $E(\infty)$, η_i and τ_i ,

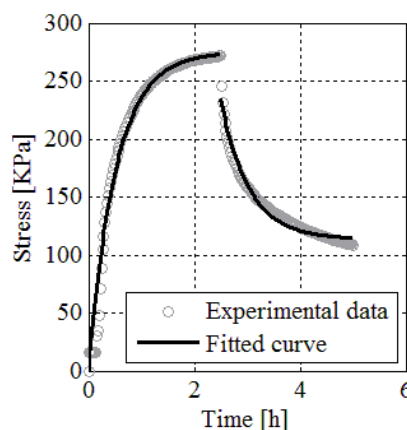


Fig. 4. Stress σ of the Sample Loaded to 50% Deformation for the Standard Linear Solid Models.

may be approximated by the following equations

$$R_1 = \frac{1}{2} \frac{\partial f(E(\infty), \eta_i, \tau_i)}{\partial E(\infty)} = 0, R_2 = \frac{1}{2} \frac{\partial f(E(\infty), \eta_i, \tau_i)}{\partial \eta_i} = 0, R_3 = \frac{1}{2} \frac{\partial f(E(\infty), \eta_i, \tau_i)}{\partial \tau_i} = 0 \quad (14)$$

where the residuals are denoted by R_1 , R_{2i} and R_{3i} . The nonlinear equations listed above, totally $2k+1$, may be iteratively solved with the function 'lsqcurvefit' provided by the software MATLAB R2011b. The obtained coefficients with the curve-fitting method (lsqcurvefit) may best fit the material model of Eq. (5) to the experiment data, although these coefficients are not unique and even result in an incorrect physical interpretation of elastic modulus because negative values are possible. These unknown coefficients, therefore, are bounded to be positive. And the initial trial values affect greatly the solutions to these unknowns, which may tend to be unreasonably infinite if the initial trial values are far away from the real solutions. The initial trial values are chosen to insure that the elastic modulus, the magnitude of which may be approximated by the quotient of the stress and the strain, is finite and positive. In this way, the unknown coefficients are iteratively solved in Eq. (14).

The continuity of curves requires that Eq. (8) and Eq. (9) satisfy the following conditions

$$\sigma(t_{0-}) = \sigma(t_{0+}) \quad (15)$$

Therefore,

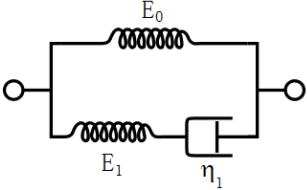
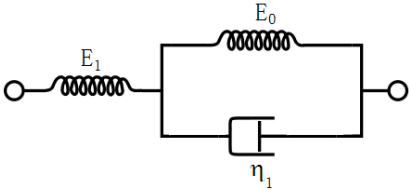
$$E(\infty)\epsilon_0 + \sum_{i=1}^k \eta_i \epsilon_0 \left[1 - \exp\left(-\frac{t_0-t_0}{\tau_i}\right) \right] = \left[E(\infty) + \sum_{i=1}^k \frac{\eta_i}{\tau_i} \right] \epsilon_0 \quad (16)$$

The equation above represents the continuity condition of the fitted curves.

Standard Linear Solid Models

The fitting functions are defined by the standard linear solid models in Prony series listed in Table 1 during the constant strain rate loading and the stress relaxation, which may be written as:

Table 1. The Standard Linear Solid Models and the Solution to the Stress Tensor.

Schematic Model		
Stress-strain Relationship	$\sigma + \frac{\eta_1}{E_1} \dot{\sigma} = E_0 \varepsilon + \frac{\eta_1 (E_1 + E_0)}{E_1} \dot{\varepsilon}$	$\sigma + \frac{\eta_1}{E_1 + E_0} \dot{\sigma} = \frac{E_1 E_0}{E_1 + E_0} \varepsilon + \frac{\eta_1 E_1}{E_1 + E_0} \dot{\varepsilon}$
Constant Strain Rate Loading	$\sigma = \eta_1 \dot{\varepsilon} \left(1 - e^{-\frac{E_1 t}{\eta_1}} \right) + E_0 \dot{\varepsilon} t$	$\sigma = \frac{E_1^2}{(E_1 + E_0)^2} \dot{\varepsilon} \eta_1 \left(1 - e^{-\frac{E_1 + E_0 t}{\eta_1}} \right) + \frac{E_1 E_0}{E_1 + E_0} \dot{\varepsilon} t$
Stress Relaxation	$\sigma = (\sigma_0 - E_0 \varepsilon_0) e^{-\frac{E_1 (t-t_0)}{\eta_1}} + E_0 \varepsilon_0$	$\sigma = \frac{E_1 E_0}{E_1 + E_0} \varepsilon_0 - \frac{E_1^2}{(E_1 + E_0)^2} \dot{\varepsilon} \eta_1 \left(e^{-\frac{E_1 + E_0 t}{\eta_1}} - e^{-\frac{E_1 + E_0 (t-t_0)}{\eta_1}} \right)$
Relaxation Time	$\tau_1 = \frac{\eta_1}{E_1}$	$\tau_1 = \frac{\eta_1}{E_1 + E_0}$

$$\sigma = \begin{cases} E \left(\dot{\varepsilon} t \right) + \eta_1 \dot{\varepsilon} \left[1 - \exp \left(-\frac{t}{\tau_1} \right) \right] & \text{constant strain rate loading} \\ E \left(\varepsilon - \varepsilon_0 \right) + \eta_1 \exp \left(-\frac{t-t_0}{\tau_1} \right) & \text{stress relaxation} \end{cases} \quad (17)$$

The goal is to find three unknown parameters, $E(\infty)$, η_1 and τ_1 . The fitting functions are defined by the standard linear solid models expressed by Eq. (12). The piecewise curve-fitting method is used, with which the load steps, the constant strain rate loading and the stress relaxation are fitted separately. The errors are calculated in each single load step. Accordingly, the corresponding coefficients are obtained. The starting trial values are evaluated by the initial elastic modulus, which are given by:

$$E(\infty)_0 = 100 \text{ [kPa]}, \eta_{1,0} = 1 \text{ [kPa/h]}, \tau_{1,0} = 0.1 \text{ [h]} \quad (18)$$

The units are omitted in the following derivations in order for simplification. The coefficients in Eq. (12) for the constant strain rate loading may be solved iteratively in Eq. (14) as

$$E(\infty) = 1.000, \eta_1 = 1368.623, \tau_1 = 0.516 \quad (19)$$

Therefore,

$$E_1 = \eta_1 / \tau_1 = 2650.322, E(0) = E(\infty) + \sum_{i=1}^k E_i = 2651.322, \alpha_1 = E_1 / E(0) = 0.9996 \quad (20)$$

Similarly, those coefficients for the stress relaxation may also be obtained

$$E(\infty) = 227.169, \eta_1 = 131.872, \tau_1 = 0.543 \quad (21)$$

Therefore,

$$E_1 = \eta_1 / \tau_1 = 242.907, E(0) = E(\infty) + \sum_{i=1}^k E_i = 470.077, \alpha_1 = E_1 / E(0) = 0.517 \quad (22)$$

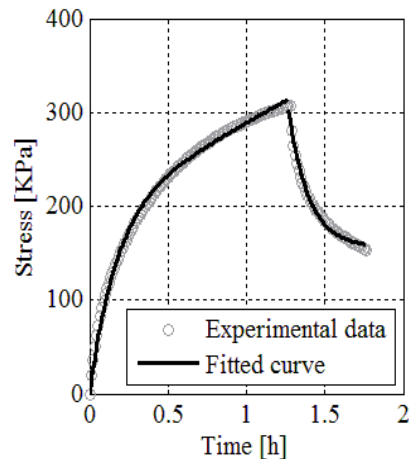


Fig. 5. Stress σ of the Sample Loaded to 25.6466% Deformation for the Standard Linear Solid Models.

Iteration may stop if the final change in the sum of squares (Eq. (13)) relative to its initial value is less than the default value of the tolerance. The fitted curve and experiment data are shown in Fig. 4, which are piecewise continuous. A high goodness of fit of the fitted curves and experimental results may be found in each load step in Fig. 4, although the continuity between fitted curves is really hard to achieve and discontinuity exists at some points.

The second sample was loaded to 25.6466% deformations. The curve-fitting results are compared with the experimental ones as shown in Fig. 5. Discontinuity exists between the loading curve and the stress relaxation stage. The material parameters at the loading stage are:

$$E(\infty) = 462.911, \eta_1 = 978.539, \tau_1 = 0.170, \quad (23)$$

$$E_1 = 5772.79, E(0) = 6235.705, \alpha_1 = 0.926$$

and the parameters for the stress relaxation are:

$$E(\infty) = 608.079, \eta_1 = 74.983, \tau_1 = 0.1310 \quad (24)$$

$$E_1 = 572.322, E(0) = 1180.401, \alpha_1 = 0.485$$

Standard Linear Solid Models

The model given by Eq. (17) may result in some defects, such as discontinuity in Figs. 4 and 5, which may be improved by substitution of Eq. (11) for Eq. (17)

$$\sigma = \begin{cases} E(\infty)\dot{\epsilon}t + \eta_1\dot{\epsilon}\left[1 - \exp\left(-\frac{t}{\tau_1}\right)\right] & \text{constant strain rate loading} \\ \left(\sigma_0 - \frac{\eta_1}{\tau_1}\right)\left[1 - \exp\left(-\frac{t-t_0}{\tau_1}\right)\right] + \frac{\eta_1}{\tau_1} & \text{stress relaxation} \end{cases} \quad (25)$$

Piecewise Curve-Fitting Method

The piecewise curve-fitting method is adopted and the fitted curve is shown in Fig. 6, where the parameters at the constant strain rate loading stage are

$$E(\infty) = 1.000, \eta_1 = 1368.623, \tau_1 = 0.516 \quad (26)$$

and

$$E_1 = \eta_1 / \tau_1 = 2650.322, E(0) = E(\infty) + \sum_{i=1}^k E_i = 2651.322, \alpha_1 = E_1 / E(0) = 0.9996 \quad (27)$$

The parameters for the stress relaxation are

$$\eta_1 = 104.943, \tau_1 = 0.345 \quad (28)$$

The elastic modulus, $E(\infty)$, may be solved in Eq. (11) as

$$E(\infty) = \left(\sigma_0 - \frac{\eta_1}{\tau_1}\right) / \epsilon_0 = 239.453 \quad (29)$$

Therefore,

$$E_1 = \eta_1 / \tau_1 = 303.873, E(0) = E(\infty) + \sum_{i=1}^k E_i = 543.326, \alpha_1 = E_1 / E(0) = 0.559 \quad (30)$$

The time history of the stress shown in Fig. 6 compared with Fig. 4, exhibits a high goodness of fit than the others. The reason is that the initial stress state σ_0 in Eq. (10) is assumed to be known for the material model defined by Eq. (25). There is still difference between those elastic modulus obtained in Eqs. (26) and (29), which may cause divergent problems for numerical solution of the model.

The time history of the stress in Figs. 5 and 7 well fits the experimental results, although there is discontinuity in the curves during the loading stage and the stress relaxation stage. The fitted parameters at the loading stage are

$$E(\infty) = 462.900, \eta_1 = 978.551, \tau_1 = 0.170, \quad (31)$$

$$E_1 = 5772.718, E(0) = 6235.618, \alpha_1 = 0.926$$

and these parameters for the stress relaxation are

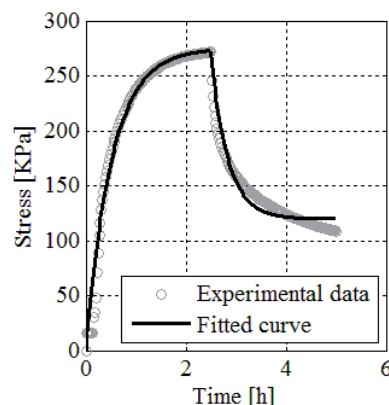


Fig. 6. Stress σ of the Sample Loaded to 50% Deformation for the Piecewise Curve-Fitting Method.

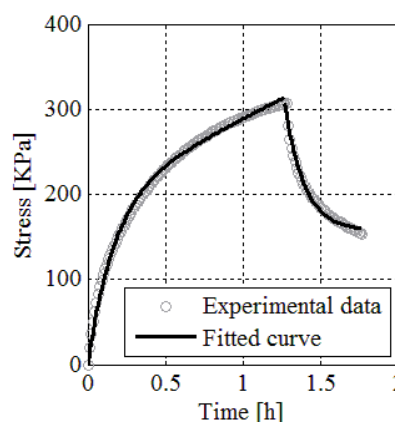


Fig. 7. Stress σ of the Sample Loaded to 25.6466% Deformation for the Piecewise Curve-Fitting Method.

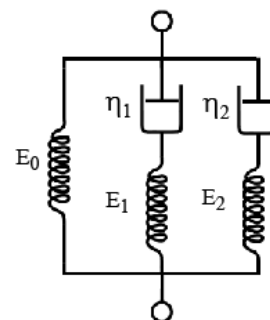


Fig. 8. Generalized Maxwell Model ($k = 2$).

$$\begin{aligned} E(\infty) &= 612.726, \eta_1 = 72.687, \tau_1 = 0.124, \\ E_1 &= 583.937, E(0) = 1196.662, \alpha_1 = 0.488 \end{aligned} \quad (32)$$

Prony Series ($k = 2$)

A more sophisticated model (Fig. 8), when the number of Maxwell element k is 2, may produce more accurate results. With the model, the constitutive relationship defined by Eqs. (8) and (12) in Prony series is selected for fitting curve.

The goal is to solve the five unknown parameters: $E(\infty)$, η_1 , τ_1 , η_2 , τ_2 , which is iteratively solved with the initial guess of the elastic modulus $E(\infty)$ and the stress in kPa. The iterative process may fail

to converge to the solutions if the predefined maximum iteration number 500 is exceeded. The relaxation time τ_2 and τ_1 may also converge to the same number since both may be linearly dependent. The iteration starts from the initial guess of the elastic modulus and the stress.

Parameters, such as α_1 , α_i , γ_i , β_1 , β_i and \mathcal{G}_i , are introduced to avoid the divergence problem presented above,

$$\begin{cases} E(\infty) = \alpha_i^2, \eta_i = \alpha_i^2, \tau_i = \gamma_i^2 & \text{constant strain rate loading} \\ E(\infty) = \beta_i^2, E_i = \beta_i^2, \tau_i = \mathcal{G}_i^2 & \text{stress relaxation} \end{cases} \quad (33)$$

Initial guesses for the relaxation time, $\tau_{1,0}$ and $\tau_{2,0}$, which may span the time range and differ initially by two or more orders of magnitude, could be

$$\tau_{1,0} = 0.1, \tau_{2,0} = 10 \quad (34)$$

The parameters of the sample loaded to 50% deformations in Fig. 9 are obtained as

$$\begin{aligned} E_\infty &= \begin{bmatrix} 0.00126 \\ 0.223 \end{bmatrix}, \eta_1 = \begin{bmatrix} 4.874e-7 \\ 8.976e-6 \end{bmatrix}, \tau_1 = \begin{bmatrix} 0.0001 \\ 0.0001 \end{bmatrix}, \\ E_1 &= \begin{bmatrix} 0.00487 \\ 0.0898 \end{bmatrix}, \alpha_1 = \begin{bmatrix} 0.00183 \\ 0.165 \end{bmatrix}, E_2 = \begin{bmatrix} 2.651 \\ 0.230 \end{bmatrix}, \\ E(0) &= \begin{bmatrix} 2.657 \\ 0.543 \end{bmatrix}, \alpha_2 = \begin{bmatrix} 0.998 \\ 0.424 \end{bmatrix}, \tau_2 = \begin{bmatrix} 0.516 \\ 0.615 \end{bmatrix} \end{aligned} \quad (35)$$

where the first row of the matrix is the parameters at the loading stage and the second row is the parameters for the stress relaxation.

The parameters of the sample loaded to 25.6466% deformations (Fig. 10) are also written in matrix form

$$\begin{aligned} E_\infty &= \begin{bmatrix} 0.446 \\ 0.482 \end{bmatrix}, \eta_1 = \begin{bmatrix} 0.979 \\ 0.0158 \end{bmatrix}, \tau_1 = \begin{bmatrix} 0.170 \\ 0.0513 \end{bmatrix}, \\ E_1 &= \begin{bmatrix} 5.769 \\ 0.307 \end{bmatrix}, \alpha_1 = \begin{bmatrix} 0.926 \\ 0.251 \end{bmatrix}, E_2 = \begin{bmatrix} 0.0168 \\ 0.434 \end{bmatrix}, \\ E(0) &= \begin{bmatrix} 6.232 \\ 1.224 \end{bmatrix}, \alpha_2 = \begin{bmatrix} 0.00269 \\ 0.355 \end{bmatrix}, \tau_2 = \begin{bmatrix} 2933.838 \\ 0.377 \end{bmatrix} \end{aligned} \quad (36)$$

As a result, the generalized Maxwell model with two Maxwell elements fits better than others, which is clearly illustrated in Figs. 9 and 10.

Numerical Analysis

The Finite element method is used to simulate the crack sealants between two pieces of cement concrete with the size of 50 mm × 50 mm × 15 mm in Fig. 11, the modeling of which is constructed with the software ANSYS 14.0.

Material Parameters

Material parameters of the generalized Maxwell model shown in Fig. 8 are chosen from the results of curve-fitting in Fig. 9 and Fig. 10. The elastic modulus $E(0)$, the relative modulus α_i and the relaxation time τ_i are input into the material model under loading till 50% deformation.

- The parameters at the constant strain rate loading are given in Eq. (35)

$$\begin{aligned} E(0) &= 2.657 [MPa], \alpha_1 = 0.00183, \tau_1 = 0.0001 [h] \\ \alpha_2 &= 0.998, \tau_2 = 0.516 [h] \end{aligned} \quad (37)$$

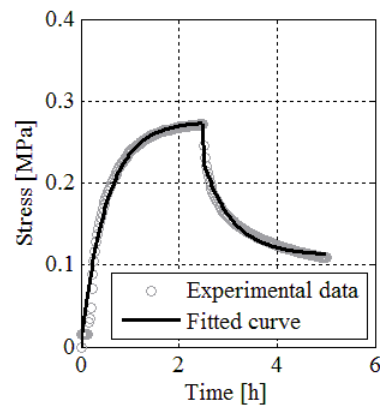


Fig. 9. Stress σ of the Sample Loaded to 50% Deformation for the Generalized Maxwell Model ($k=2$).

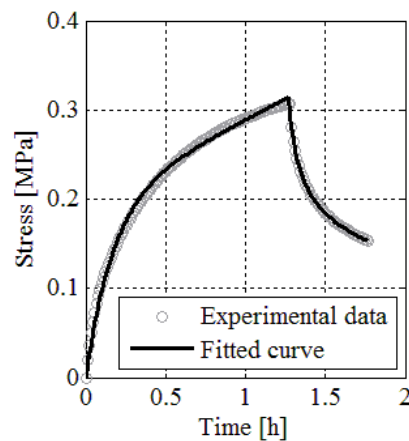


Fig. 10. Stress σ of the Sample Loaded to 25.6466% Deformation for the Generalized Maxwell Model ($k = 2$).

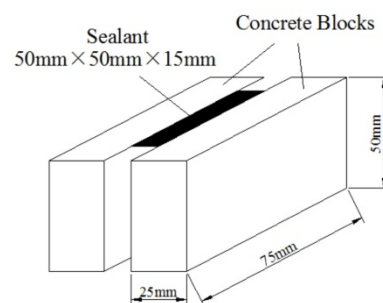


Fig. 11. Test Specimen.

- and those for the stress relaxation

$$E(0) = 0.543[\text{MPa}], \alpha_1 = 0.165, \tau_1 = 0.0001[\text{h}] \quad (38)$$

$$\alpha_2 = 0.424, \tau_2 = 0.615[\text{h}]$$

Poisson's ratio is assumed to be constant, that is 0.35. The shear modulus and the bulk modulus may be evaluated by

$$G(t) = \frac{E(t)}{2(1+\mu)}, K(t) = \frac{E(t)}{3(1-2\mu)} \quad (39)$$

Computational Model

Due to the symmetric properties of the geometry and the boundary conditions, only one-eighth of the model in Fig. 11 is built and meshed. Finer mesh is not recommended since the geometrical size of the computational model is as small as 25 mm × 25 mm × 7.5 mm, which are meshed with the 20-node brick element (solid186 in ANSYS). The element size is set by half of the width, which is 3.75 mm as shown in Fig. 12(a).

The boundary conditions are defined on the surface of the geometric model. The left, the back and the bottom surfaces are assumed to be symmetric planes, where the displacements in the normal directions are constrained as show in Fig. 12(b). The right side surface is assumed to be seamlessly adhered to the surface of the concrete and the displacements along the X-axis and the Z-axis are zero, shown in Fig. 12(b). The displacements along the Y-axis are set on the right side surface according to the experiment process, during which the displacements are defined by the constant strain rate loading until the strain reaches 0.5, as is shown in Fig. 2.

Geometric nonlinearity is assumed for the modeling of the crack sealants under the constant strain rate loading and the stress relaxation. The material model with the stress-time relationship, which is taken to be continuous, is selected according to the curve-fitting method. The large deformation and the small strain are computed. Furthermore, the line search technique is introduced to the Newton-Raphson method to improve the iteration process.

Numerical Results of the Sample Loading to 50% Deformation

Modeling of crack sealants under the constant strain rate loading and the stress relaxation (Fig. 2) is solved with the finite element method. The displacement on the right surface in Fig. 12(b) increases with time till 3.75 mm and crack sealants under the constant strain rate are numerically simulated. The displacements on the right surface are then assumed to be constant (3.75 mm). The initial stress during the second load step is assumed to be the one obtained at the end of the constant strain rate loading period, which is input to determine how crack sealants release the stress under the constant strain. Material properties are also changed and the stress relaxation is solved afterwards.

Only one eighth of the model is simulated because of the symmetrical properties of the geometry and the boundary conditions. The deformations after the constant strain rate loading are illustrated

in Fig. 13, where the deformation of the geometrical model is compared with the undeformed one (Fig. 13(a)). The displacements along the Y-axis, X-axis and Z-axis are shown in Fig. 13(b), (c), and (d), respectively. Contour plots of the displacements in Fig. 13(b), (c), and (d) show that the displacements in the normal directions on the symmetric planes are zero.

The principle stress σ_1 and σ_3 are shown in Fig. 14, where stress concentration may be found in the corners. Time history of the stress σ_y at the constant strain rate loading is surveyed at the point

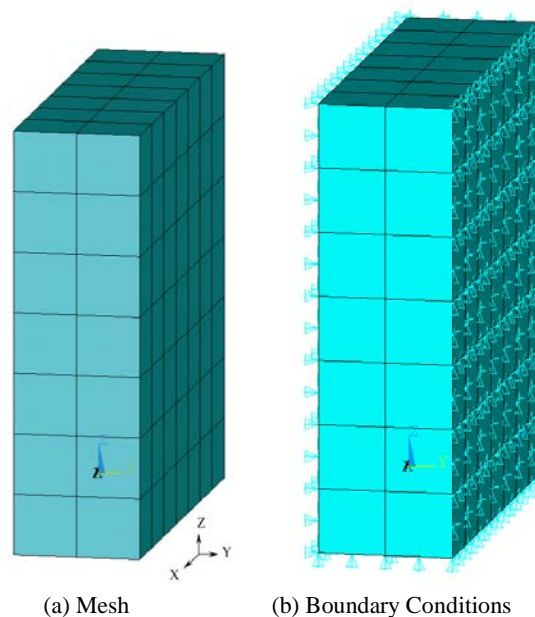


Fig. 12. Mesh and Boundary Conditions.

(0, 0, 3.75) on the right side surface to determine whether the selected material model conforms to the experimental observations. Numerical results are comparable with the experimental ones illustrated in Fig. 15 except that the stress at the end of the constant strain rate loading period relaxes due to the short relaxation time with its maximum value of 0.516 h obtained with the curve-fitting method.

Relaxation of the initial stress, which is assumed to be the stress at the end of the constant strain rate loading period, is studied. Boundary conditions of the displacements along the normal direction on the symmetrical planes are set as zero. The displacements along the Y-axis on the right plane are kept as the one at the first loading period, namely 3.75 mm.

The stress also decreases with time (Fig. 15). The starting time point t_0 for the stress relaxation is the one at the end of the first loading period, which is treated as the origin in time dimension for the analysis of the stress relaxation. Material parameters are estimated in Eq. (38). The numerical results σ_y at the point (0, 0, 3.75) are compared with the experimental ones, which supports conclusion that the generalized Maxwell model (a spring connected with two Maxwell elements in parallel) perfectly describes the material characteristics during the stress relaxation.

The same example is simulated except that the material model is defined by the standard linear model (Eq. (17)) in order to compare the numerical results with the ones of the generalized Maxwell

model shown in Fig. 8. The numerical results of both models illustrated in Figs. 15 and 16 are comparable with the experimental results at the loading stage, though the stress solved with the generalized Maxwell model in Fig. 15 fits better than the one of the standard linear model for the stress relaxation in Fig. 16.

Numerical Results of the Sample Loaded to 25.6466% Deformation

The sample loaded to 25.6466% deformation is simulated. Material parameters of the generalized Maxwell model shown in Fig. 8

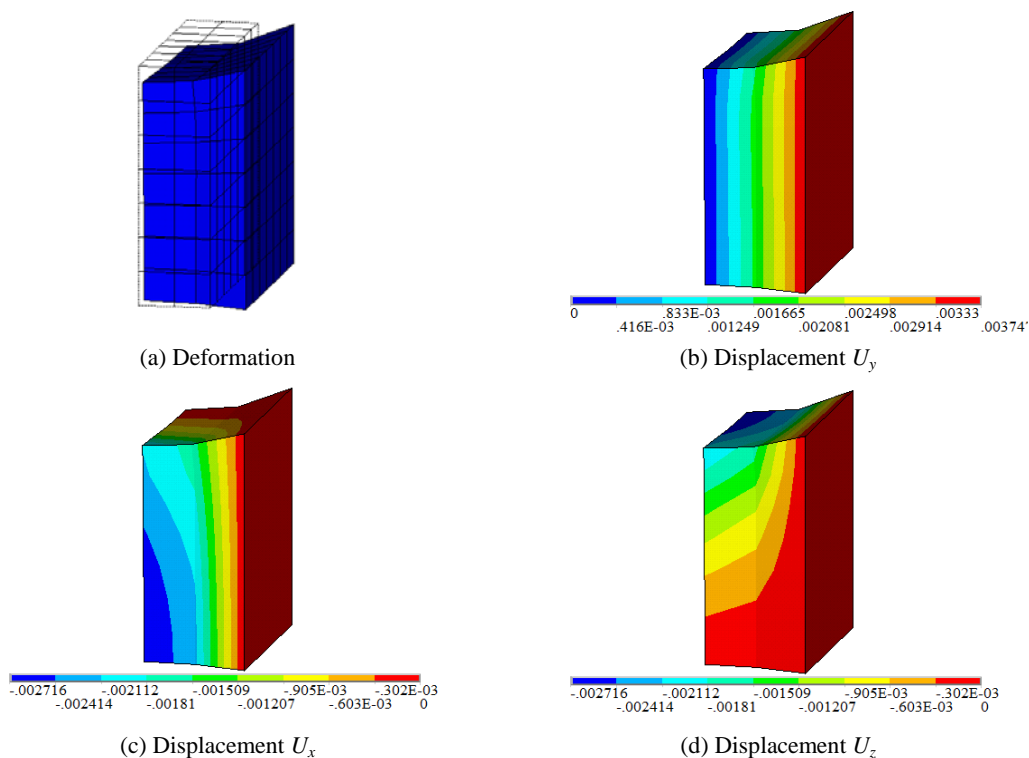


Fig. 13. Deformed Shape and Contour of Displacement Tensor for the Sample Loaded to 50% Deformation.

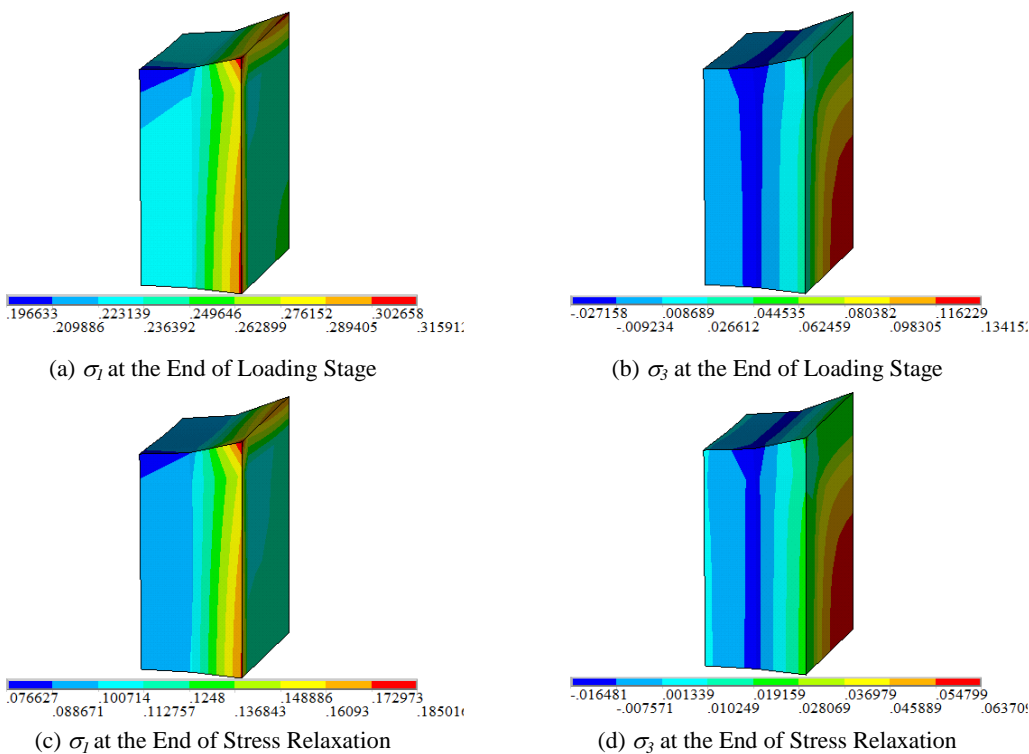


Fig. 14. Principle Stress σ_1 and σ_3 for the Sample Loaded to 50% Deformation.

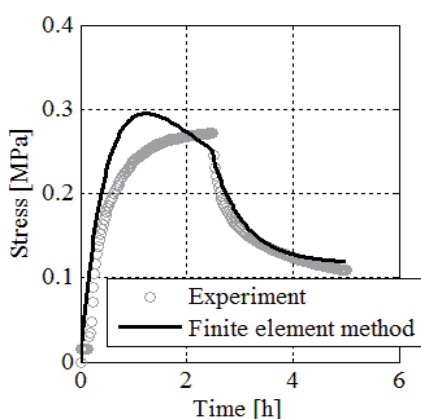


Fig. 15. Time History of the Stress σ_Y Solved with the Generalized Maxwell Model.

are curve-fitting results given in Eq. (36), where

- the parameters at the constant strain rate loading are

$$E(0) = 6.232[MPa], \alpha_1 = 0.926, \tau_1 = 0.170[h] \tag{41}$$

$$\alpha_2 = 0.00269, \tau_2 = 2933.838[h]$$

- and those for the stress relaxation are

$$E(0) = 1.224[MPa], \alpha_1 = 0.251, \tau_1 = 0.0513[h] \tag{42}$$

$$\alpha_2 = 0.355, \tau_2 = 0.377[h]$$

Only one eighth of the model is simulated with the finite element method because of the symmetrical properties of the geometry and the boundary conditions. Boundary conditions for the displacement

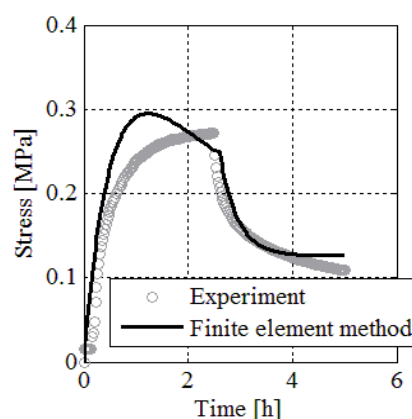


Fig. 16. Time History of the Stress σ_Y Solved with the Standard Linear Model.

on the right side surface increases with time till 1.924 mm and then assumed to be kept constant (1.924 mm).

The deformations after the constant strain rate loading are illustrated in Fig. 17, where the deformations of the geometrical model are compared with the undeformed ones (Fig. 13 (a)). The displacements along the Y-axis, X-axis and Z-axis are shown in Fig. 13(b), (c), and (d), respectively. Contour plots of the displacements in Fig. 13(b), (c), and (d) shows that the displacements in the normal directions on the symmetric planes are zero.

The deformation and the principle stress of the test sample under loading till 25.6466% deformation in Figs. 17 and 18 is similar to that under loading till 50% deformation in Figs. 13 and 14, where stress concentration may be found in the corners. Time history of the stress σ_x is surveyed at the point (0, 0, 3.75), of which numerical

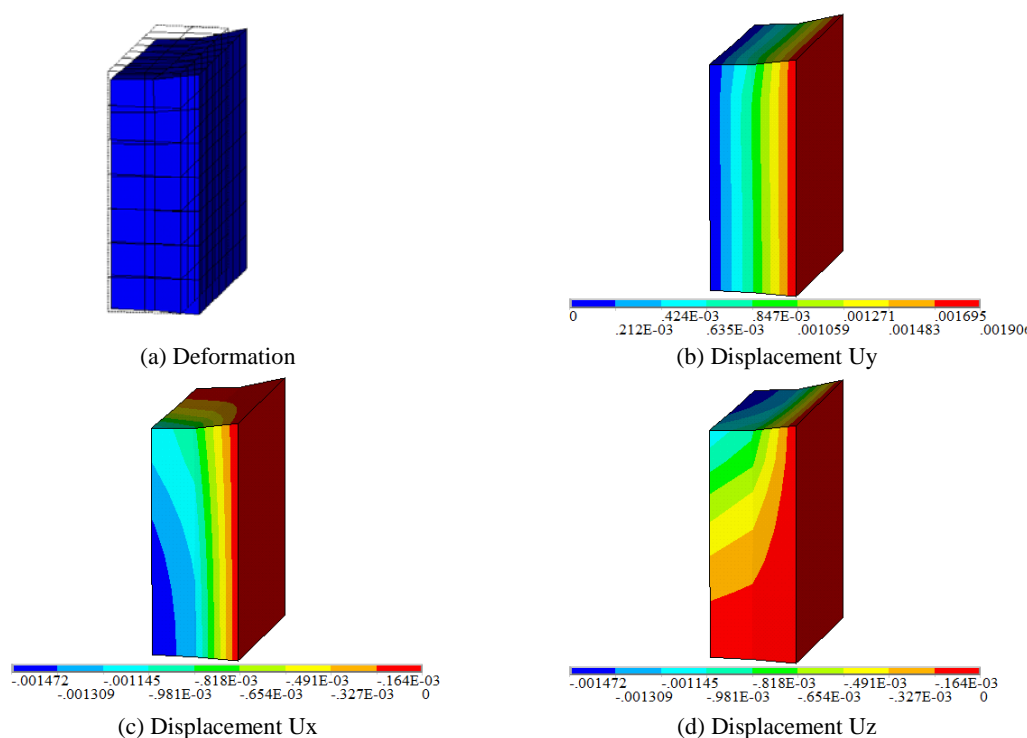


Fig. 17. Deformed Shape and Contour of Displacement Tensor for the Sample Loaded to 25.6466% Deformation.

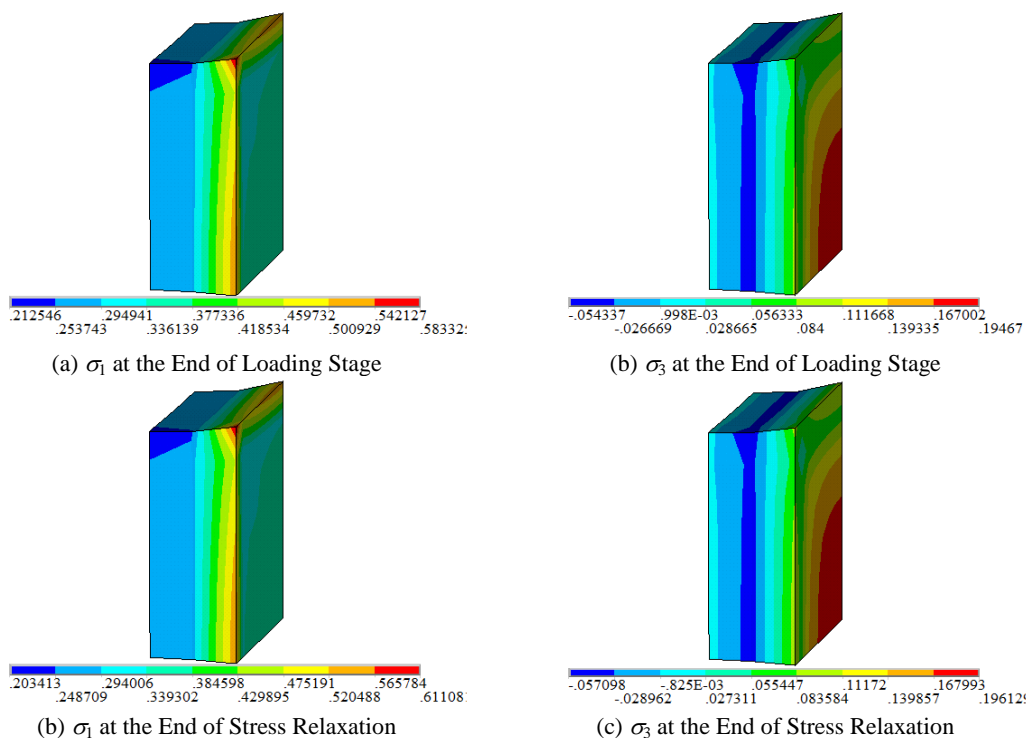


Fig. 18. Principle Stress σ_1 and σ_3 for the Sample Loading to 25.6466% Deformation.

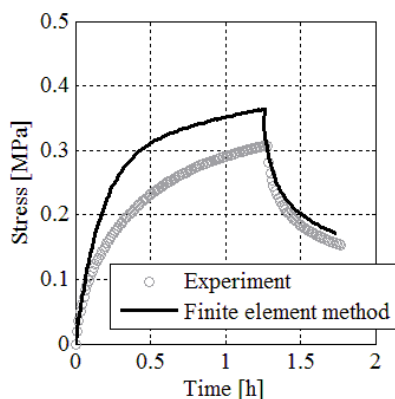


Fig. 19. Time History of Stress σ_y for the Sample Loaded to 25.6466% Deformation.

results are comparable with the experimental ones illustrated in Fig. 19 except for the loading stage.

Conclusions

The generalized Maxwell model is chosen for curve-fitting to determine the material model for sealant. Comparison of fitted curve and experimental results proves that the generalized Maxwell model in Prony series is well suited for describing the experimental process. Moreover, finite element method with material model defined by the generalized Maxwell model in Prony series is introduced for numerical solution of tension and stress-relaxation of the crack sealants. By comparison of the numerical results with the experimental ones, this paper demonstrated that the tension and the stress-relaxation of crack sealants may be accurately depicted by the generalized Maxwell model.

Numerical solutions with the generalized Maxwell model capture all of the important qualitative properties of the experimental data except a slight discrepancy between numerical results and experimental ones. The discrepancy arises from the facts that the fitted curve cannot perfectly fit the experimental results. The continuous curve of the stress-strain relationship is necessary for the numerical solution with the finite element method while the piecewise curve fitting method always produces discontinuity in the fitted curves. The constant strain rate loading and the stress relaxation may be well simulated with the material parameters introduced in the piecewise curve fitting method.

Acknowledgements

This study was supported by National Natural Science Foundation of China (No.51378242, 51008146), the Ministry of Science and Technology of China (No. 2013DFA81910), the Science and Technology Project of the Department of Transportation of Hebei Province (No. Y-2014015), and the Transportation Industry Science and Technology Project of Beijing (No. kj2013-2-14). The authors would like to acknowledge their financial support.

References

1. Galehouse, L., King, H., Leach, D.R., Moulthrop, J., and Ballou, B. (2005). Preventive maintenance treatment performance at 14 years. Transportation Research Board, *92nd Annual Meeting Compendium*, Washington, DC, USA.
2. Yang, S.H., Al-Qadi, I.L., McGraw, J., Masson, J.F., and McGhee, K.M. (2010). Thresholds identification and field validation of the performance based guidelines for the selection of hot-poured crack sealants. Transportation

- Research Board, *89th Annual Meeting Compendium*, Washington, DC, USA.
3. Masson, J.F., Collins, P., Margeson, J., Margeson, J., and Polomark G. (2002). Analysis of bituminous crack sealants by physico-chemical methods and its relationship to field performance. Transportation Research Board, *81st Annual Meeting Compendium*, Washington, DC, USA.
 4. Carter, S., Ksaibati, K., Huntington, G. (2005). Field and laboratory evaluations of hot-poured thermoelastic bituminous crack sealing of asphalt pavements. Transportation Research Board, *84th Annual Meeting Compendium*, Washington, DC, USA.
 5. ASTM D5329-09 (2009). Standard test methods for sealants and fillers, hot-applied, for joints and cracks in asphaltic and Portland cement concrete pavements, *Annual Book of ASTM Standards*, ASTM International, West Conshohocken, PA, USA.
 6. ASTM D6690-06a (2006). Standard specification for joint and crack sealants, hot-applied, for concrete and asphalt pavements, *Annual Book of ASTM Standards*, ASTM International, West Conshohocken, PA, USA.
 7. Ministry of Transport of China, JT/T 740-2009 (2009). Specification for hot-applied crack sealants for asphalt pavements. *China Communications Press*, Beijing, China (in Chinese).
 8. Al-Qadi, I.L., Loulizi, A., Aref, S., and Masson, J.F. (2005). Modification of bending beam rheometer specimen for low-temperature evaluation of bituminous crack sealants. *Transportation Research Record*, 1933, pp. 97-106.
 9. Al-Qadi, I.L., Yang, S.H., Dessouky, S., and Masson, J.F. (2007). Low temperature characterization of hot poured crack sealant using modified SHRP direct tensile tester. Transportation Research Board, *86th Annual Meeting Compendium*, Washington, DC, USA.
 10. Al-Qadi, I.L., Fini, E.H., Masson, J.F., and McGhee, K.M. (2008). Effect of bituminous material rheology on its adhesion. Transportation Research Board, *87th Annual Meeting Compendium*, Washington, DC, USA.
 11. Soliman, H. and Shalaby, A. (2007). Evaluation of joint and crack sealants based on cyclic loading and rheological properties. *2007 Annual Conference of the Transportation Association of Canada (TAC)*, Saskatoon, Canada, pp. 1-12.
 12. Soliman, H., Shalaby, A., and Kavanagh, L. (2008). Performance evaluation of joint and crack sealants in cold climates using DSR and BBR tests. *Journal of Materials in Civil Engineering*, ASCE, 20(7), pp. 470-477.
 13. Soliman, H. and Shalaby, A. (2009). Characterizing the low-temperature performance of hot-pour bituminous sealants using glass transition temperature and dynamic stiffness modulus. *Journal of Materials in Civil Engineering*, ASCE, 21(11), pp. 688-693.
 14. Elseifi, M., Dessouky, S., Al-Qadi, I.L., and Yang S.H. (2006). A viscoelastic model to describe the mechanical response of bituminous sealants at low temperature. Transportation Research Board, *85th Annual Meeting Compendium*, Washington, DC, USA.
 15. Al-Qadi, I.L., Dessouky, S., and Yang, S.H. (2010). Linear viscoelastic modeling for hot-poured crack sealants at low temperature. *Journal of Materials in Civil Engineering*, ASCE, 22(10), pp. 996-1004.
 16. Cai, E. (1989). *Viscoelastic Mechanics Basis*. Beijing University of Aeronautics and Astronautics Press, Beijing, China (in Chinese).